Available online at www.sciencedirect.com
SCIENCE DIRECT®
Geomorphology 53 (2003) 147–164
GEOMORPHOLOGY
www.elsevier.com/locate/geomorph

Modeling large-scale fluvial erosion in geographic information systems

David P. Finlayson*, David R. Montgomery

Department of Earth and Space Sciences, University of Washington, Box 351310, Seattle, WA 98195, USA

Received 30 July 2001; received in revised form 27 June 2002; accepted 1 August 2002

Abstract

Variants of the stream power model have become standard for large-scale erosion modeling in geographic information systems (GIS) because they can be applied over broad areas without the need for detailed knowledge of stream characteristics. GIS-based implementations of the shear stress, stream power per unit length and stream power per unit area models are closely related to one another and related also to empirical sediment yield models derived from continental-scale factor analyses. Based on a detailed examination of the implementation of stream power analyses at the scale of continental mountain ranges, we demonstrate that: (1) the careful selection of a digital elevation model (DEM) projection can minimize length and area distortion when analyzing large portions of the earth (such as the Himalaya or Andes) in the two-dimensional plane of a DEM. (2) The area-discharge proxy frequently employed in GIS-based stream power studies may not be appropriate for rivers that flow through significant rain shadows or climatic zones. (3) Decreasing the resolution of a DEM from 30- to the 900-m typical for studies of large extent decreased the mean slopes of 15 rivers in the Olympic mountains by 65%, increased the mean drainage basin size by 14%, and caused a 17% reduction in median main-stem channel length. (4) The coefficients k, m and n common to different versions of the Stream Power Law are themselves sensitive to grid resolution when determined from an analysis of area–slope plots. (5) Stream power per unit area decreased in the Olympics mountains as grid resolution decreased.

Keywords: Landscape evolution; GIS; Stream power; Erosion modeling

1. Introduction

Over the past decade, the use of geographic information systems (GIS) and digital elevation models (DEMs) has become increasingly pervasive in fluvial geomorphic analysis. GIS are now widely employed in small- to medium-sized watershed studies where high-resolution DEMs can be analyzed along with databases containing land cover, hydrologic, climatic, and historical records. In particular, GIS are beginning to play a role in the analysis of continental denudation where large spatial scales (i.e., small cartographic scale ratios on a map or DEM) and data volumes preclude the use of traditional geomorphic analysis techniques (Walling and Webb, 1996; Ludwig and Probst, 1998; Montgomery et al., 2001; Finlayson et al., 2002). A growing body of literature is available to guide the application of GIS technology to landscape

* Corresponding author.
E-mail address: dfinlays@u.washington.edu (D.P. Finlayson).

0169-555X/02/$ - see front matter © 2002 Elsevier Science B.V. All rights reserved.
doi:10.1016/S0169-555X(02)00351-3

analysis (particularly fluvial studies) in small-scale areas (e.g., Gurnell and Montgomery, 1999; Maidment and Djokic, 2000). However, the adaptation of GIS to studies of continental-scales is new and little information is available that outlines the problems of working at large scales in GIS.

The productive use of GIS in large-scale studies is hindered by poor understanding of large-scale denudation processes and significant technological limitations intrinsic to GIS. Nevertheless, GIS-based approaches provide one of the few means available for systematically examining the role of spatial variability in soil properties, rock types and numerous other geologic and climatic properties in the evolution of a landscape. The spatially explicit nature of GIS analyses and the GIS emphasis on incorporating real-world data combine to make GIS a powerful tool for building insight into the evolution of complex landscapes and landscape processes.

This paper focuses on modeling large-scale fluvial erosion in continental mountain ranges. Examples of coarse-scale applications will be drawn from our experience in modeling the fluvial systems of the Himalaya (Finlayson et al., 2002). Where validation is required at higher DEM resolutions than are presently available for the Himalaya, we use the Olympic Mountain Range of Washington State. We focus on issues that are peculiar to working at large scales and avoid issues common to smaller scale studies.

2. Fluvial erosion models

The two primary approaches for modeling fluvial erosion in mountainous terrain are (i) the extrapolation of statistical models of river sediment yield parameters with forcing variables, and (ii) the physical modeling of river processes directly. Both styles of modeling were originally applied to small watersheds before the advent of GIS and have matured with the increasing power of computer technology. The statistical model, in particular, has been applied simultaneously to large portions of the earth within a GIS environment (Walling and Webb, 1996; Ludwig and Probst, 1998).

Both approaches have limitations. In the case of statistical models, the functional relationship between physical factors and the sediment yield response is heavily scale and situation dependent while, at the same time, the physical processes eroding the river bed and transporting sediment are lumped and parameterized away. Statistical models typically yield a picture of erosion that is heavily biased by modern anthropogenic impacts and the limitations of too little data collected over too short a time frame. Physical models, on the other hand, can rarely be implemented in a natural environment with any great confidence. The detailed physics of erosion and sediment transport are difficult to grapple with under controlled circumstances and can become unmanageable in natural systems, particularly mountain rivers that depart markedly from the ideal, canal-like forms assumed in conventional hydraulic formulae.

2.1. Statistical models

Early attempts to elucidate the controls on the sediment yield of world rivers were hampered by a lack of data, inadequate extrapolation procedures, and the scale-dependent nature of sediment yield data (Langbein and Schumm, 1958; Walling and Webb, 1996). Moreover, they provided little information on the spatial variability of erosion within the upstream basin (Walling and Webb, 1996). Recent efforts, however, have made extensive use of GIS technology to couple sediment yield data with hydroclimatic, biological, and geomorphological parameters (e.g., Ludwig and Probst, 1998). These empirical models help to elucidate the first-order controls on sediment yield and have been used to develop denudation maps of the continents (Walling and Webb, 1996; Ludwig and Probst, 1998).

The current estimate of the total global sediment yield is about 20 Gt a^{-1} (Milliman and Syvitski, 1992), more than 50% of which is thought to be human induced (Walling and Webb, 1996). Attempts to explain the natural variability in sediment yields have invoked mean precipitation (e.g., Langbein and Schumm, 1958; Wilson, 1973), relief (Ahnert, 1970), or various combinations of discharge, contributing area, and lithology (e.g., Jansen and Painter, 1974). Ludwig and Probst (1998), in one of the most extensive sediment yield regression analyses yet attempted, compared 21 parameters for 60 major world rivers (the basins of which encompass about 50% of the earth's continental surface). They found

that three factors best describe global suspended sediment yield:

$$Q_{ss} = 0.02(Q \times S \times P_s) \quad (1)$$

where Q_{ss} is total suspended sediment yield (t km^{-2} a^{-1}), Q is mean annual runoff (mm), S is the average basin slope, and P_s is seasonal precipitation variability (mm). Ludwig and Probst (1998) found a strong correlation between hydrologic variables, and a relatively weak negative correlation between sediment yield and drainage basin size. Overall, Eq. (1) resulted in an average global sediment yield of 139.4 t km^{-2} a^{-1} with a total sediment flux of 14.8 Gt a^{-1}, about 75% of world estimate by Milliman and Syvitski (1992).

2.2. Physical models

Fundamentally, the rate of river incision into bedrock is a function of the basal shear stress of the river:

$$\tau_b = -\gamma R \frac{dE}{dx} \quad (2)$$

where τ_b is the basal shear stress, γ is the specific weight of water, R is the hydraulic radius and dE/dx is the energy grade line of the channel, which in uniform flow is equivalent to the channel slope (Chow, 1959). Particle motion begins when the effective bed shear stress (τ') exceeds the critical shear stress for grain motion (τ_c):

$$q_b = k(\tau' - \tau_c)^n \quad (3)$$

where q_b is the bed load transport capacity, and k and n are empirical values. τ' is the portion of the basal shear stress (τ_b) corrected for momentum losses caused by hydraulic roughness:

$$\tau' = \tau_b - \tau'' - \tau''' - \cdots - \tau^n \quad (4)$$

where $\tau'' - \cdots - \tau^n$ are the momentum losses due to gravel bars, woody debris, boulder obstructions, and so on (e.g., Buffington and Montgomery, 1999).

While local calculations of Eq. (3) are possible in a GIS analysis in practice, the detailed information required for evaluating Eq. (4) is rarely available. In addition, the critical shear stress that must be overcome for particle motion has a wide range for natural mountain rivers (Buffington and Montgomery, 1997). The problem of erosion into bedrock is even more complex, as the effects of corrosion, corrasion, and cavitation combine to work against the electrochemical forces that bind a rock together (Knighton, 1998) thereby complicating the definition of τ_c considerably. In addition, the critical shear stress required to erode bedrock is greater than that for incipient motion of sediment cover (Costa and O'Connor, 1995), but how much greater remains poorly constrained and is likely to vary considerably.

2.3. Stream power

As an alternative to the first-principles approach to river incision and the statistical models presented above, a number of closely related and more-or-less simplistic models have emerged that attempt to relate river incision (ε) to basal shear stress (τ_b) or some function of stream power (Ω) (Howard, 1998; Sklar and Dietrich, 1998; Stock and Montgomery, 1999; Whipple and Tucker, 1999). After normal substitutions, most of these models become quite similar and are collectively known as *Stream Power Laws* of river incision.

The stream power equations make extensive use of the concept of *hydraulic geometry* first introduced by Leopold and Maddock (1953). Downstream hydraulic geometry equations characterize empirical power law relationships between the discharge of a river, Q, and river parameters, v, such as channel width or depth:

$$v = cQ^d \quad (5)$$

where c and d are fitting parameters. As discharge is a function of drainage area, it has become common practice in DEM applications to adopt an area-discharge proxy ($Q = aA^h$) in hydraulic geometry relations to yield:

$$v = cA^d \quad (6)$$

The use of hydraulic geometry relationships and the area-discharge proxy in fluvial analyses based on DEMs has the advantage that river parameters such as width and depth are rendered independent of the spatial resolution of the DEM. Hence, a 1-km resolution DEM grid does not restrict the analytical

representation of river channels to a minimum or maximum width of 1 km. Many studies have shown that hydraulic geometry equations perform acceptably for alluvial rivers (e.g., Leopold and Maddock, 1953; Carlston, 1969), but few have parameterized Eq. (6) in mountainous terrain (e.g., Montgomery and Gran, 2001). Nevertheless, we shall adopt the common practice of invoking hydraulic geometry relations in our analyses as needed to estimate mountain river parameters that have not been, or cannot be measured directly from a DEM.

The shear stress version of the Stream Power Law was first introduced to model badland evolution of coastal plains in the State of Virginia (Howard and Kerby, 1983) and has since been widely applied to bedrock river incision in mountains:

$$\dot{\varepsilon} = -k_1 \tau_b^b \tag{7}$$

where $\dot{\varepsilon}$ is the river incision rate, k_1 is the *coefficient of erodibility*, and b is a positive constant. Standard substitutions that make Eq. (7) more tractable than physical models based on Eq. (3) include the hydraulic geometry-based approximation for the hydraulic radius of the channel (Leopold and Maddock, 1953):

$$R \approx d = cA^f \tag{8}$$

where d is the channel depth, A is the cumulative drainage area, c and f are positive constants; and an approximation for the energy grade line of the channel that, under uniform conditions, is approximately equal to the channel gradient (S):

$$\frac{\mathrm{d}E}{\mathrm{d}x} = S. \tag{9}$$

Substituting Eqs. (2), (8) and (9) into Eq. (7) yields:

$$\dot{\varepsilon} = k_1 (\gamma c)^b A^{f+b} S^b \tag{10}$$

A similar approach is to relate $\dot{\varepsilon}$ to the stream power per unit length of channel (Ω):

$$\Omega = \gamma QS \tag{11}$$

The stream power per unit area or specific stream power (ω) can be obtained by dividing Eq. (11) through by the width of the channel (w):

$$\omega = \frac{\Omega}{w} \tag{12}$$

Here again, the practice is to simplify Eqs. (11) and (12) by using hydraulic geometry relations to substitute for discharge ($Q = aA^h$) and channel width ($w = sA^e$). For both the case of stream power per unit length:

$$\dot{\varepsilon} = C\Omega \; = C\gamma QS \tag{13}$$

$$= (C\gamma a) A^h S \tag{14}$$

and for specific stream power:

$$\dot{\varepsilon} = \frac{C\Omega}{w} = \frac{C\gamma QS}{sA^e} = \frac{C\gamma a A^h S}{sA^e} \tag{15}$$

$$= \left(\frac{C\gamma a}{s}\right) A^{h/e} S^n \tag{16}$$

where s and e are constants. Eqs (10), (14) and (16) all share the same general form of:

$$\dot{\varepsilon} = kA^m S^n \tag{17}$$

where k, m, and n are constants.

A great deal of energy has been expended attempting to parameterize Eq. (17) for various environments. Accounting for typical values of h, e, f and b, standard values of the exponents m and n are considered to be $m = 1$, $n = 1$ for stream power per unit length models; $m = 1/2$, $n = 1$ for a specific stream power model; and $m = 1/2$ and $n = 2/3$ for a shear stress model (Whipple and Tucker, 1999), while values of k can vary over several orders of magnitude (Stock and Montgomery, 1999).

The generalized Stream Power Law (Eq. (17)) is based on Eq. (2) which attempts to characterize the basic physical processes thought to be driving erosion in a river system, but in practice, the physical meaning of the equation is obscured by the numerous coefficients making up k, m and n. Eq. (17) does not model any of the factors responsible for momentum loss (and which thereby reduce τ_b to τ') (Howard, 1998; Sklar and Dietrich, 1998); k is dimensional and

thus scale dependent (Whipple and Tucker, 1999) as well as widely variable with lithology and environment (Stock and Montgomery, 1999); and the unit stream power version rests on a series of assumptions about hydraulic geometry supported by relatively sparse data from mountainous terrain (Montgomery and Gran, 2001). What limited success this equation has had in modeling real river systems may owe as much to its similarity with Eq. (1) as to any foundation in first principal physics. Even if this concern proves warranted, there are few alternative erosion models that can be applied systematically to continental-scale landscapes.

3. Digital elevation model resolution

Early enthusiasm for GIS-based geomorphic analysis was dampened by the sober reality that hydrologic modeling using DEMs is strongly affected by use of coarse grid sizes that cannot resolve fine-scale landscape features (Zhang and Montgomery, 1994; Walker and Willgoose, 1999). The acquisition of high-resolution topography improves the situation for engineers working in small watersheds, but it does relatively little for geomorphologists working with continental landscapes who must cope with the cost of increasing resolution, particularly if a full suite of tectonic and climatic models must also be coupled. The balance between computational efficiency and the desire for finer resolution data must also include the considerable time required to prepare a DEM for hydrologic modeling (Garbrecht and Martz, 2000; Saunders, 2000). In addition, large-scale analyses compound the distortion inherent in representing the earth in the planar format of DEMs.

The following sections deal with cartographic and measurement scale and how they effect GIS implementations of erosion models. The first section examines how map projections affect length and area measurements and presents an example analysis for determining the error involved with two common projections in order to minimize the distortion over the area of interest. The second looks at the cost of coarse grid resolution on the representation of watershed boundaries, slope, and river long profile length.

3.1. Map projection

The large spatial extent of the analyses considered in this paper pushes the ability of DEMs to represent an ellipsoidal earth. Raster DEMs or grids are a regular two-dimensional matrix of elevations. Hence, grids suffer the same distortion problems inherent to representing the earth as traditional two-dimensional maps. It is necessary to carefully select a map projection in order to minimize distortions in distance and area throughout an analysis region. While GIS packages greatly simplify the transformation of data into suitable projections, it is worth examining the details of this process because the poor choice of projection can compromise an analysis, while a judicious one can minimize the loss of accuracy, even over vast territories. For example, the US Geological Survey using an Albers projection with standard parallels at 29°30′ and 45°30′ has plotted the contiguous states of the United States of America with a maximum scale error of only 1.25% (McDonnell, 1979). It is possible to do considerably worse with a poor choice of projection.

Prior to projection, a GIS typically assumes an ellipsoidal approximation to the surface of the earth and the elevation data is projected onto the plane of the DEM via any one of a number of classical map projection formula (Snyder, 1987). For our purposes, it will greatly simplify the discussion of map projection properties to assume that the world is a perfect sphere where the surface area equals that of the earth. The distortion involved in this spherical approximation (relative to an ellipsoidal approximation) of the earth is relatively small compared to the typical distortion incurred by projecting the spheroid onto a plane, but it is not discussed below (see Snyder, 1987 for a formal treatment of map projection properties and formulae).

The length distortion factor (Hradílek and Hamilton, 1973), or scale factor (McDonnell, 1979), sf, of a unit length PP_1 on a sphere mapped onto a plane is:

$$\mathrm{sf} = \frac{P'P_1'}{PP_1} = \frac{\text{map length}}{\text{sphere length}} \tag{18}$$

To understand how distortion affects a single point on the GIS raster, we employed Tissot's Indicatrix

where a differentially small circle on a sphere is projected onto a plane. The resulting shape is always an ellipse. The ratio of the lengths of the semimajor axis, a, and the semiminor axis, b, of this ellipse represents the maximum and minimum distortion at the point being considered (Hradílek and Hamilton, 1973; McDonnell, 1979). If the ellipse is circular ($a = b$), the projection is conformal; if the ellipse has an area equal to that of the generating circle, the projection is equal-area; finally, if either a or b is constant, the projection is equal-distant in the corresponding direction. For many common map projections, a and b occur along the meridians and parallels of the earth making it relatively easy to calculate the scale factors associated with length, area, and angle. It should be remembered that no projection of a sphere onto a plane can preserve both shape and area simultaneously.

To illustrate the effect of map projections on the scale of a raster grid, consider the Himalayan mountains and vicinity as shown in Fig. 1 clipped from the GTOPO30 DEM of the world (US Geological Survey, 1996). The data are delivered in the cylindrical equidistant projection or plate carrée (Fig. 1A). The plate carrée projection is standard (sf = 1) along the Equator and all meridians, but parallels are exaggerated by $1/\cos\phi$, where ϕ is latitude, so that they are always the same length as the Equator, even at the poles. Hence, the semimajor axis of Tissot's indicatrix (a) aligns with the parallels of the plate carrée projection, while the semiminor axis (b) aligns with the meridians. The

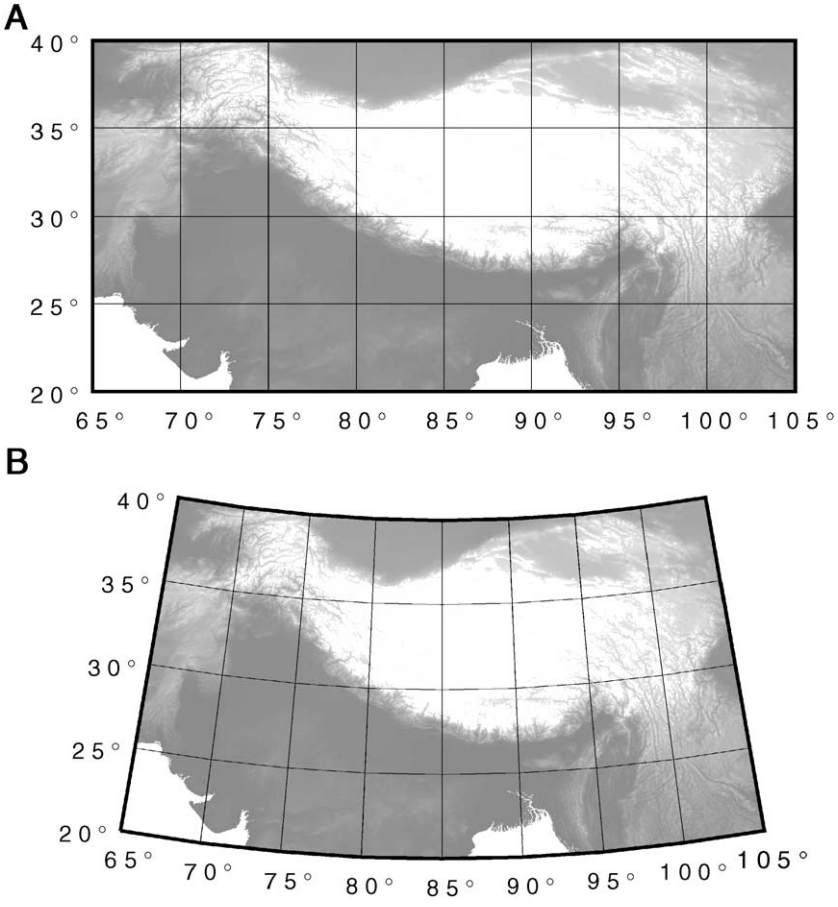

Fig 1. Map projections of Northern India, the Himalaya and the Tibetan Plateau. A portion of the GTOPO30 DEM of Asia is shown in (A) the cylindrical equidistant projection (plate carrée) and (B) a conic equal-area with two standard parallels (Albers) located at 35°N and 25°N. Black is low elevation, white is high.

maximum and minimum length distortion factors a and b (Eq. (18)) for the plate carrée projection are:

$$a = \frac{2\pi R \times 1/\cos\phi}{2\pi R} = \sec\phi \tag{19}$$

$$b = \frac{2\pi R}{2\pi R} = 1 \tag{20}$$

$$a \times b = \sec\phi \tag{21}$$

where R is the radius of the earth. The length of 1° (in kilometers) along a parallel is plotted against a sphere with a radius of 6370 km in Fig. 2A along with resulting maximum and minimum scale factor a (Fig. 2B). Because the minimum length distortion b is everywhere equal to 1, the area distortion in the plate carrée projection (Eq. (21)) is everywhere equal to $a = \sec\phi$. For the latitude range shown in Fig. 1A (20–40°N) and highlighted in gray in Fig. 2, the minimum scale factor is 1.064 (6.4% exaggeration in east–west distance and area measurements) and reaches 1.305 (30.5% exaggeration in east–west distances and area) by the northern border of the grid. This projection reaches a length and area distortion factor of 2 ($a = 2$) at a latitude of ± 60° and becomes infinite at the poles.

In order to reduce the east–west scale exaggeration in the area of the Himalaya and southern Tibet, the grid in Fig. 1A can be projected into an Albers equal-

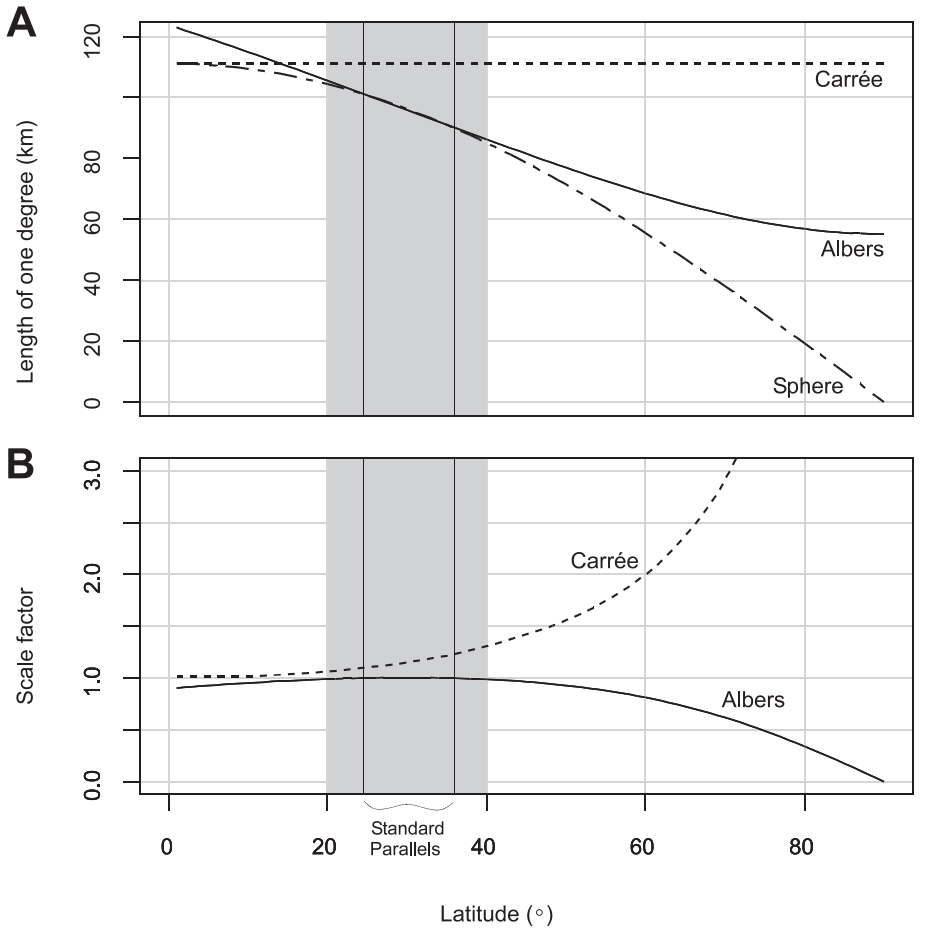

Fig. 2. Map projection properties. (A) The length of 1° along a parallel of the earth (spherical approximation) is compared to the length of 1° along a parallel of the map projections of Fig. 1A and B. (B) The scale factor (sf) between each map projection and a spherical approximation of the earth. The latitude range (shown in gray) and the standard parallels are the same as in Fig. 1.

area projection with standard parallels located at 35° and 25° (Fig. 1B). The Albers projection has the following maximum and minimum distortion properties (Hradílek and Hamilton, 1973):

$$a = \frac{1}{\sqrt{2n}} \frac{\sin\delta}{\sqrt{C - \cos\delta}} \tag{22}$$

$$b = \frac{\sqrt{2n}\sqrt{C - \cos\delta}}{\sin\delta} \tag{23}$$

$$a \times b = 1 \text{ (equal area)} \tag{24}$$

where δ is the colatitude $(90 - \phi)$; and the constants n and C are defined as follows:

$$n = \frac{(\cos\delta_2 - \cos\delta_1)}{2} \tag{25}$$

$$C = \frac{(\cos\delta_2 - \cos\delta_1)(1 + \cos\delta_1\delta_2)}{(\cos\delta_2 - \cos\delta_1)(\cos\delta_2 + \cos\delta_1)} \tag{26}$$

where δ_1 and δ_2 are the colatitudes of the lower and upper standard parallels, respectively (35° and 25° in the Himalayan case). Figs. 1B and 2B show the resulting raster and maximum length distortion a for this projection. Between the standard parallels, the Albers projection has a maximum length distortion factor of 1.004 (0.4%) at 30°7′ and is never greater than 0.0127 (1.27%) within the latitude range shown. It also has the desirable properties that it is equal-area ($a \times b = 1$) and not too far from conformal ($a \approx b$).

This demonstration is not to say that the conic equal-area (Albers) projection is inherently better than the cylindrical equidistant (plate carrée) for GIS purposes. Rather, our point is that the choice of projection must be considered when GIS analysis is attempted on data sets with large spatial extent. In fact, if the study area were chosen to be near the Equator, the plate carrée would have performed better than the Albers; and both projections would entail significant distortion if the study region were aligned along a meridian as are the Andes Mountains of South America, where a Transverse Mercator projection might work well. It is important to recognize the inherent limitations of the raster plane for

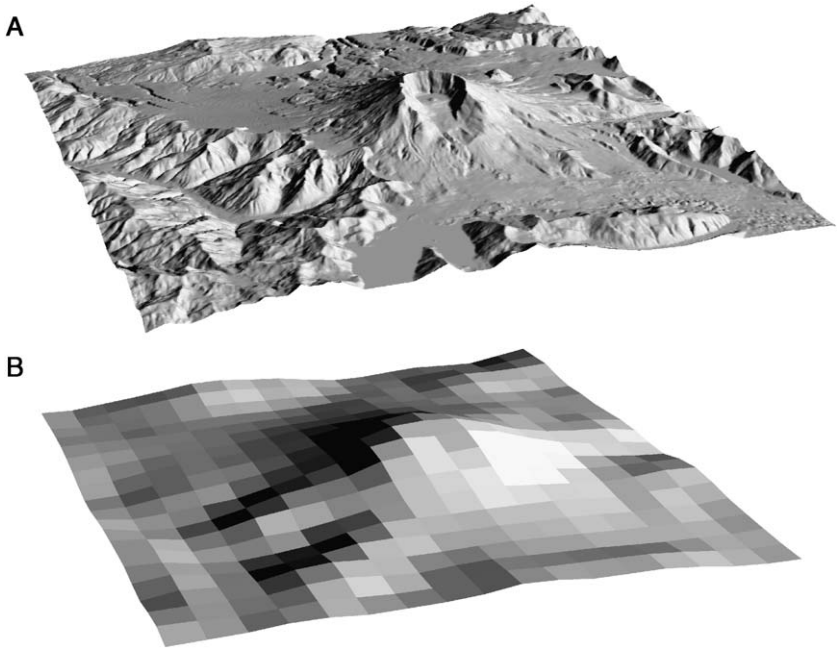

Fig. 3. Shaded relief maps of Mt. St. Helens, Washington State, generated from 30- and 900-m resolution DEMs. Thirty-meter resolution topography (A) has greater detail than can be depicted here; whereas 900-m resolution topography (B) maintains only a crude approximation of the volcano [no vertical exaggeration in the figure].

large-scale analysis and to explicitly account for the distortion in area and distance measure in geomorphic analysis.

An important caveat about raster projection is that the process of transforming coordinate systems will almost always necessitate re-sampling of the raster grid. The plate carrée projection of GTOPO30, for example, fits naturally within the orthogonal Cartesian axes of the raster matrix; but the Albers projection utilizes a radial (polar) coordinate system. The projected data must be re-sampled onto a Cartesian grid using some form of interpolation scheme. Re-sampling affects data fidelity, such that it may be prudent to handle the scale distortions through the use of look-up tables or directly within measurement algorithms rather than re-projecting the data from the outset. This is particularly true if the original grid has already received significant processing (such as drainage network enforcement) that would be lost during the re-sample step of grid projection or would otherwise be time consuming or expensive to restore.

3.2. Slope, area and length

The analysis of very large areas in GIS frequently involves the use of relatively low-resolution spatial databases. Often this is the result of a lack of available information at higher resolutions. However, this situation can result from a compromise between resolution and computational efficiency, particularly if the analysis is performed in preparation for, or as part of, a dynamically coupled geomorphic–tectonic model. In either case, grid-cell resolution affects the statistical properties of several important hydrologic and geomorphic indices. Hence, application of the Stream Power Law (Eq. (17)) to large landscapes suffers from

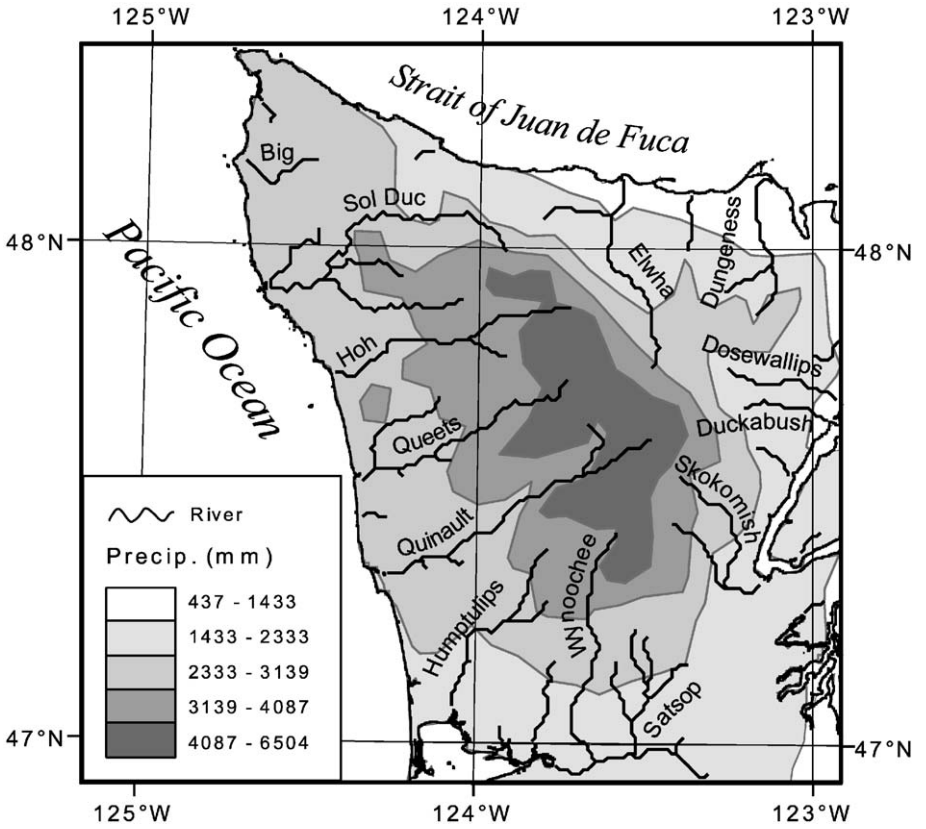

Fig. 4. Major rivers and generalized precipitation field of the Olympic Mountains, Washington State. The 15 major watersheds of the Olympics encompass a total surface area of just over 10,300 km^2. Precipitation data generalized from Daly et al. (1994).

scale issues in the representation of the landscape within the GIS.

The cost in spatial resolution of re-sampling a 30-m DEM of Mt. St. Helens, Washington to a 1000-m cell size is illustrated in Fig. 3. Clearly, the loss of detailed topographic information is severe, and hydrographic characteristics derived from such a coarse grid contain nothing but the strongest regional patterns. Nevertheless, this coarse resolution is typical of landscape evolution models, and there is a need to scale what we have learned from small watersheds to continental river systems.

Several studies have examined the effect of grid cell resolution on drainage area and slope and found that slope decreases with decreasing grid size (Zhang and Montgomery, 1994; Hammer et al., 1995; Walker and Willgoose, 1999; Zhang et al., 1999) while drainage area increases (Zhang and Montgomery, 1994; Walker and Willgoose, 1999). Comanor et al. (2000) analyzed a low-resolution global data set of continental watersheds and river networks (Grahm et al., 1999) and reported that, while most drainage basins were within 50% of their actual basin size, some basins were off by more than 100%.

We re-sampled USGS 30-m DEMs of the Olympic Peninsula to create 90- and 900-m DEMs (Fig. 4) by assigning to each low-resolution cell the mean elevation value of the 30-m data it replaced. The surface area of the 15 watersheds we examined was slightly larger than 10,000 km^2, significantly smaller than the drainage basins of large continental rivers (for example, the mountainous portion of the Indus River drainage basin shown in Fig. 5, covers 9.7×10^5 km^2). However, the 30-m data for the Olympic Mountains are much better than public domain data of many large mountain ranges.

Averaging the results of the 15 basins (Fig. 6), we found a 65% decrease in mean, main-stem river slope when moving from 30- to 900-m data and a 14% average increase in drainage area. However, the mean increase in drainage area was heavily influenced by two river basins that absorbed their smallest neighbors as the grid size increased. This had little effect on the rest of the range where both the median drainage area and the distribution of the drainage areas increased slightly (Fig. 6). In addition, we calculated a median decrease in river length of 17%. We repeated the above analysis with a high resolution, 10-m DEM for the two largest rivers of the Olympics, the Elwha and the Quinault. When moving from a 10-m DEM long profile to one derived from a 900-m DEM, the Quinault and Elwha Rivers lost 26% and 14% of their length, respectively.

It is tempting from this analysis to suggest a simple scaling factor that would adjust the results of low-

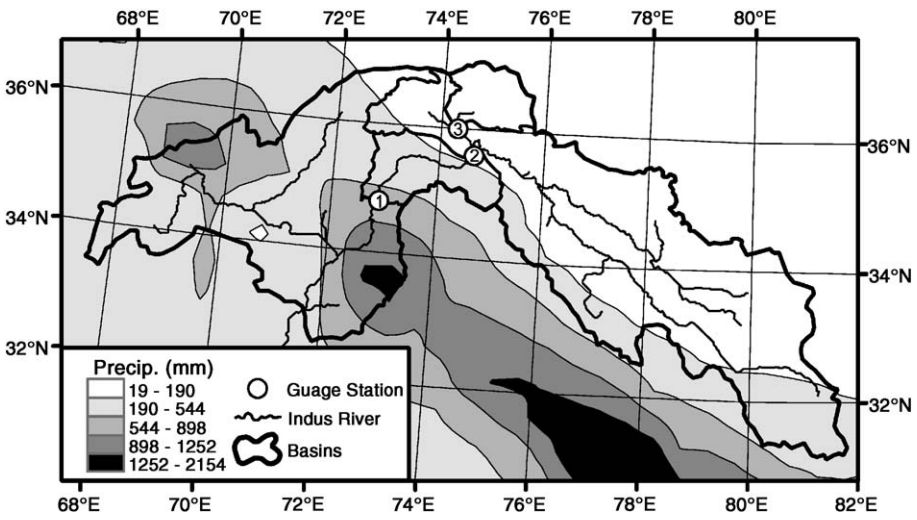

Fig. 5. Himalayan portion of the Indus River drainage basin (above 250-m elevation) and generalized precipitation field. The Indus watershed has been divided into three sub-basins based on the location of published discharge data (Collins, 1996). Alpha values used in Eq. (28) are 3.05, 1.64 and 16.8 for stations 1, 2, and 3, respectively. Precipitation data generalized from Leemans and Cramer (1991).

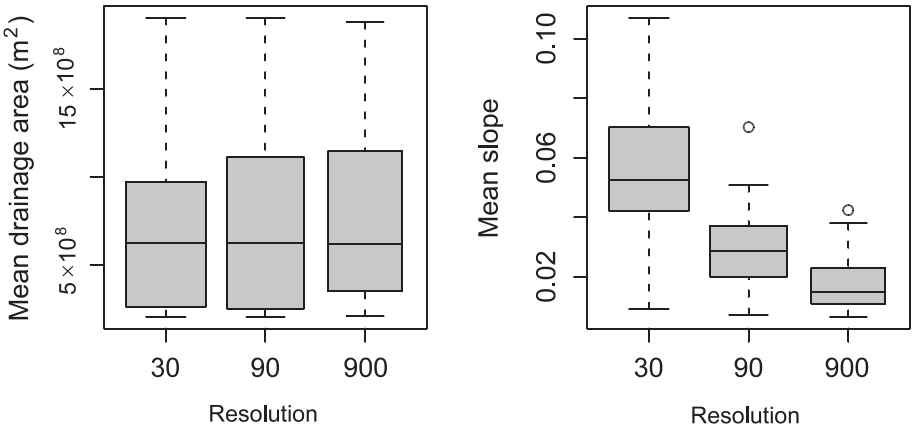

Fig. 6. Drainage area and slope as a function of resolution for composite distributions of measurements from the long profiles of the 15 largest rivers in the Olympic Mountains. The central horizontal line represents the median value of all profiles; the top and bottom of the box represent the 75th and 25th percentile of the data, the interquartile range (IQR), respectively; and the top and bottom whiskers mark the location of data points no more than 1.5 times the IQR from the median value. Data points outside of this range are marked individually. As a function of decreasing resolution, the mean drainage area of the 15 rivers increased by 14% while mean slope decreased by 65%.

resolution analysis of slope and drainage area so that they more closely resemble high-resolution characteristics. However, Zhang et al. (1999) found that for slope, at least, a single fractal parameter could not span the full range of grid resolutions considered here. This may indicate that scaling properties are unique for each location and that high-resolution data must be used to generate the appropriate scale factor for low-resolution derivatives. Alternatively, it may be evidence of polygenetic topographic evolution where different surface processes and time scales produce multi-fractal geomorphology.

4. Application of stream power in GIS

The following sections address issues of direct relevance to the implementation of erosion modeling using the Stream Power Law in GIS systems. The first concerns the area-discharge proxy that is in common use in both analytical and computer applications. The second discusses the parameterization of the stream power constants and how these appear to be scale dependent.

4.1. The area-discharge proxy

The calculation of discharge plays a significant role in the Stream Power Law because it can attain very large values compared to slope, and hence dominate Eq. (17). However, the calculation of river flow is a complex problem that is highly specific to location and time. Further, the specific relationships between discharge and erosion processes are not well established. It has become common practice to try and simplify the calculations by attempting to model only the most significant or effective discharge (typically, the bankfull discharge) or to substitute a surrogate for discharge —such as drainage area— that is easier to calculate over an entire drainage basin (Howard, 1998; Sklar and Dietrich, 1998; Stock and Montgomery, 1999; Whipple and Tucker, 1999). However, the simple area-discharge proxy may not always be appropriate at continental scales.

Drainage area is often used as a proxy for discharge in erosion models because of the paucity of discharge data available for many world rivers. To first order, the area-discharge proxy ($Q = aA^h$) works well for many small- to mid-sized watersheds in the United States. For example, we analyzed the 1659 gauging stations found in the HCDN stream flow database (Slack and Landwehr, 1992) and found that drainage area explains 61% of the variation in mean annual maximum discharge with a simple log-linear formula (Fig. 7):

$$Q = 0.92A^{0.70} \quad (27)$$

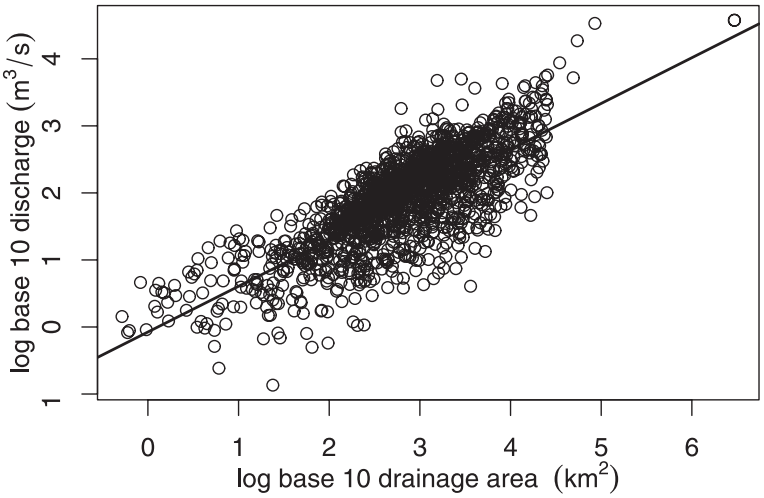

Fig. 7. Mean annual maximum discharge as a function of cumulative drainage area for the 1659 drainage basins defined by the HCDN data set (Slack and Landwehr, 1992). The least-squares regression equation is $Q = 0.92A^{0.70}$ with an $R^2 = 0.61$.

with Q in m^3/s and A in km^2. The exponent of 0.7 found here for gauged locations on rivers throughout the continental United States is similar to exponent values reported for downstream trends along individual rivers (0.7–1.0) (Dunne and Leopold, 1978; Knighton, 1987). However, does the area-discharge proxy hold for large, continental rivers? For example, the Indus (Fig. 5) and Tsangpo/Brahmaputra Rivers begin in the dry Tibetan plateau and flow through hundreds of kilometers of alpine desert before turning south onto the monsoon drenched flanks of the range. Other large rivers throughout the world cross significant climatic zones or rain shadows where it may be incorrect to assume that each parcel of land contributes uniformly to the river discharge.

Fortunately, there is little computational difference in a GIS between calculating cumulative drainage area and calculating a precipitation-weighted cumulative area and this can be used to estimate runoff and discharge. For example, discharge at a cell i, can be modeled on a DEM as the weighted sum of n individual contributing cells j:

$$Q_i = \sum_{j=1}^{n} (\alpha_j A_j P_j) \tag{28}$$

where A is the cell area (m^2), P is the precipitation falling in each cell (m a^{-1}), and α is a calibration coefficient. Wherever cell i has a known discharge Q, for example, at a gauging station, it is possible to set α for all upstream contributing cells j such that $Q_i = Q$, (e.g., Finlayson et al., 2002). If sufficient gauging data is available, it is possible to model the discharge of the river reasonably well. However, even if no discharge measurements are available to calibrate α in Eq. (28), it may still be better to set $\alpha = 1$and use Eq. (28) as a relative measure of discharge throughout a river course rather than resorting to a hydraulic geometry proxy such as Eq. (27) (we use this approach for the Olympics below). The advantage of calculating discharge from Eq. (28) over using equations like Eq. (27) is that the GIS can begin to capture the spatial variability in discharge that would otherwise be lost if one were to use a uniform area-discharge proxy.

We performed the above analysis for the 16 largest watersheds of the Himalaya using the GTOPO30 DEM (USGS, 1996), the IIASA worldwide climate database (Leemans and Cramer, 1991), and various sources for gauging data (see Finlayson et al., 2002). We show the results here only for the Indus River (Fig. 5), the calibration of which relied primarily on three river discharge measurements from Collins (1996). We first calculated Q_i for each cell in the GTOPO30 DEM of the Indus watershed by Eq. (28) using $\alpha = 1$. We next determined the contributing area above each of the published discharge measurements

from Collins (1996) (shown in Fig. 5) and calculated an α coefficient for all grid cells i in these sub-basins that would increase or decrease Q_i at the measurement location so that it matched the published values. Note that the sub-basins are nested, so that setting α in an upper basin affects the discharge of the downstream basins. The results of this discharge model are compared to the standard cumulative drainage area model in Fig. 8. Also in Fig. 8, we show the results of a similar comparison for a very small river (the Big River) in the Olympic mountains. No gauging data is available for the Big River, hence α is set equal to 1 in Eq. (28) for the entire Big River drainage basin.

For the Indus River, drainage area grows much faster than modeled discharge (Fig. 8) and so the area-discharge proxy likely over estimates river dis-

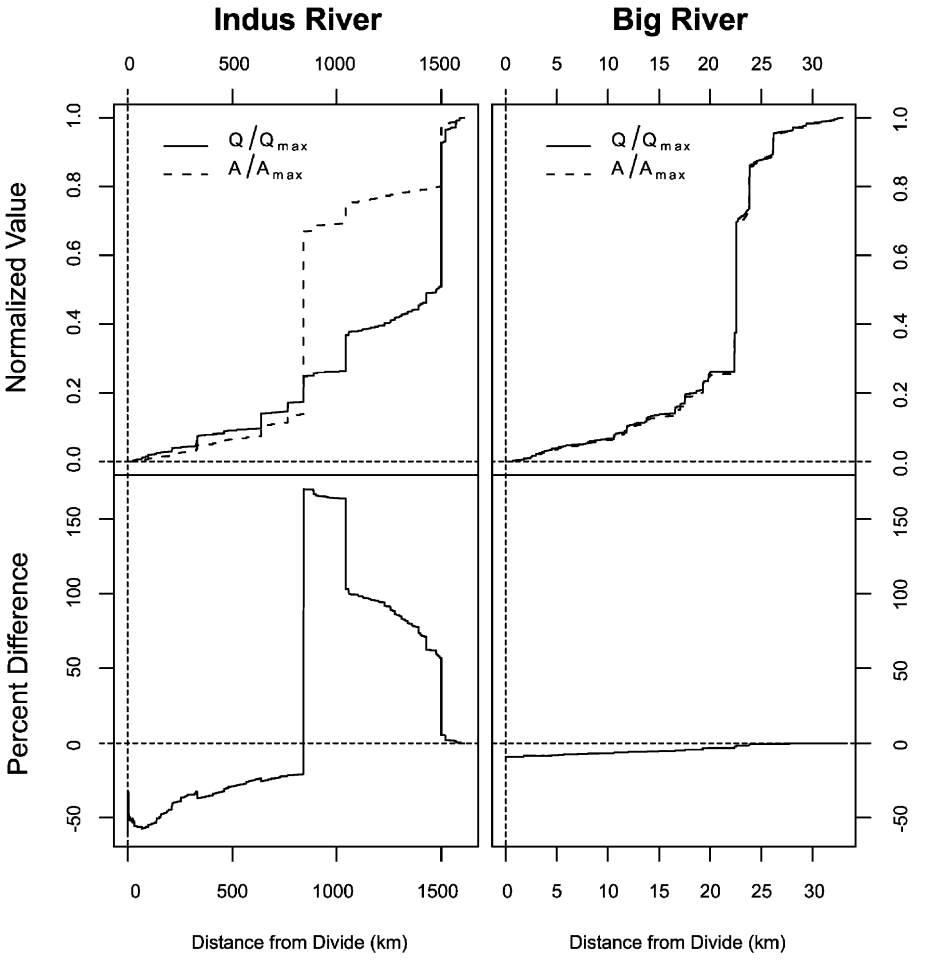

Fig. 8. Comparison of modeled river discharge to cumulative drainage area. The graph compares normalized modeled discharge to normalized drainage area for a large river (Indus River, Pakistan) and a small river (Big River, Olympic Peninsula, Washington State) to assess how well drainage area performs as a proxy for annual river discharge. The upper plot in the left panel shows the normalized drainage area (A/A_{max}) and normalized discharge (Q/Q_{max}) of the Indus River as a function of distance from its drainage divide in kilometers. The lower plot shows the difference ratio $(A/A_{max} - Q/Q_{max})(Q/Q_{max})^{-1}$ between the normalized drainage area and normalized discharge. The drainage area and normalized discharge lines in the right panel are identical for the Big River, indicating that area is an excellent proxy for modeled discharge. This contrasts with the Indus River, where drainage area is a poor proxy for modeled river discharge with a range of error between -50% and over 150% reflecting large changes in environment throughout the course of the river.

charge by as much as 150% for a significant portion of the river's course. In contrast to this, the Big River flows through a nearly homogeneous precipitation field (Fig. 4) and shows almost perfect correlation between modeled discharge and drainage area. The area-discharge proxy should not be applied to watershed analyses where there is doubt about the uniform contribution of runoff from each cell in the model.

4.2. Stream power parameters

One of the principal difficulties with the Stream Power Law (Eq. (17)) is the proper parameterization of the constants k, m, and n. A partial solution possible in steady-state environments is to equate uplift rate ($\dot{U}$) with erosion rate ($\dot{\varepsilon}$) and then solve for drainage area as a function of slope (S):

$$\dot{\varepsilon} = \dot{U} = kA^m S^n \tag{29}$$

$$S = \left(\frac{\dot{U}}{k}\right)^{1/n} A^{-m/n} \tag{30}$$

Following Snyder et al. (2000), the value of m/n can be estimated by a power law regression of the form:

$$S = k_s A^{-\theta} \tag{31}$$

where $k_s=[\dot{U}/k]^{1/n}$ and $\theta = m/n$. Assuming steady-state, if independent information is available about one of the exponents m or n and the uplift rate is known, k

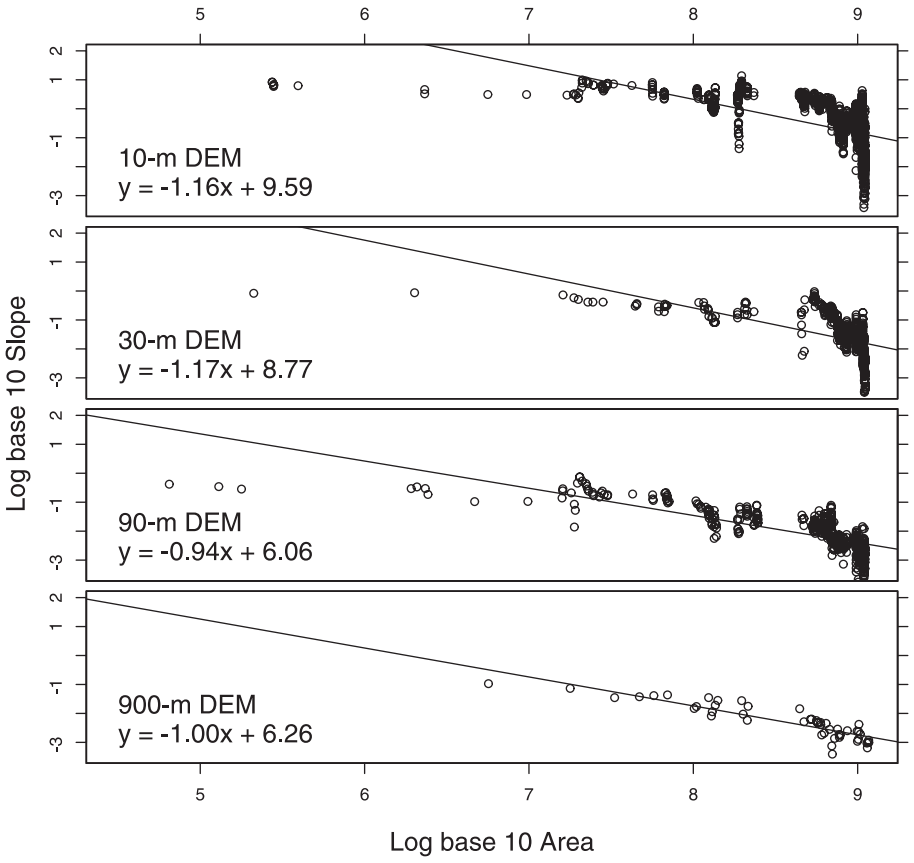

Fig. 9. The long profile of the Elwha River extracted from 10-, 30-, 90-, and 900-m DEMs illustrating the effects of grid resolution on least-squares regressions and thereby on θ and k_s. In addition to resolution effects documented in Fig. 6, the number of points available on the 900-m-long profile is significantly reduced from the 10-m profile, changing the distribution of the data and the values of the regression from which θ and k_s were calculated.

can be backed out of k_s. If the mountain range is not in steady-state or if there is strong orographic precipitation, then $\theta \neq m/n$ and the technique of Snyder et al. (2000) is not applicable for estimating m/n (Roe et al., 2002).

The Olympic Mountains are approximately in steady-state, with a long-term balance between rock uplift and erosion rates being maintained since the Miocene (Brandon et al., 1998; Pazzaglia and Brandon, 2001). We extract the long profile of the Quinault River from each of the 10-, 30-, 90-, and 900-m DEMs; filtered each profile to remove points with no slope (flat areas); plotted slope as a function of area according to Eq. (31); and fit a simple, least-squares line through all of the available data points (Fig. 9). Although Walker and Willgoose (1999) found that slope vs. area plots were not sensitive to small changes in resolution when the data were generally all of high resolution, we found that the decrease in data points defining the Elwha River channel (79 in the 900-m model vs. 9800 in the 10-m model) had a profound impact on θ and k_s. This was true of all of the profiles we examined in the Olympics. Moving from 30- to 900-m resolution, we found a mean increase in θ of 30% and a mean decrease in k_s of 51% (Fig. 10). Because of the log scaling of Fig. 9, a 51% drop in k_s changes k by more than an order of magnitude.

4.3. Stream power as a function of resolution

In order to summarize the discussion about scale and stream power, it is instructive to look at an actual stream power calculation carried out over grid resolutions of 10 to 1000 m for the Elwha River, on the Olympic Peninsula. The grids were derived from the USGS 10-m grid as described in Section 3.2. For each grid resolution, we calculated a precipitation-weighted cumulative area calculation according to Eq. (28) using annual precipitation data from Daly et al. (1994). Because there is only one gauge on the Elwha River, α is a constant for the whole basin and we chose to simplify the calculations by assuming $\alpha = 1$ everywhere.

The mean stream power ($\bar{\Omega}$) increased with decreasing resolution as each cell represents the integration of more surface area. However, normalizing for surface area, the mean stream power per unit area ($\bar{\omega}$) decreased by 66%. Although grid resolution is not a linear measure (i.e., a 10-m grid cell is 10×10 m^2), a plot of mean stream power and mean stream power per unit area as a function of resolution shows that total stream power is positively correlated with grid size, whereas stream power per unit grid-cell area is inversely correlated (Fig. 11). Hence, stream power values calculated from DEMs are scale dependent and

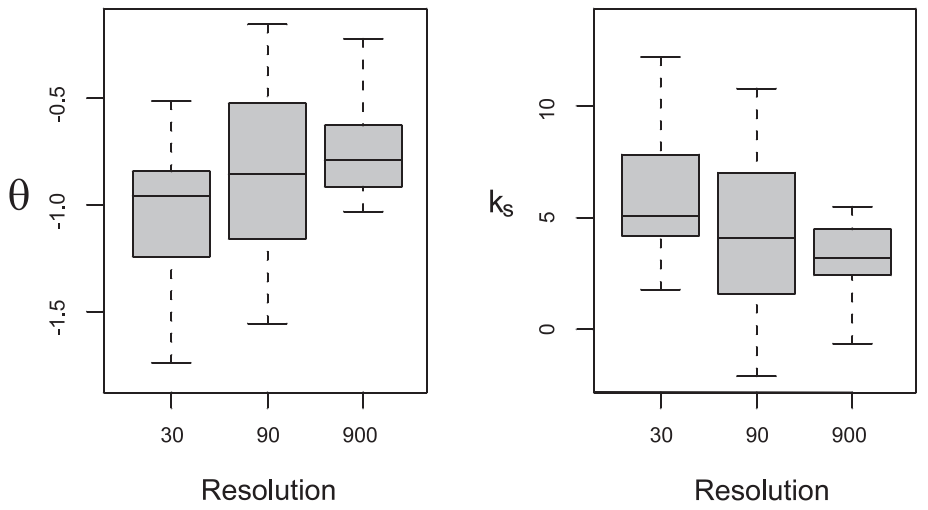

Fig. 10. Variation in θ and k_s as a function of grid resolution. Values of θ and k_s were calculated from the long profiles of the largest rivers in the Olympic Mountains. The long profiles were derived from 30-, 90-, and 900-m DEMs.

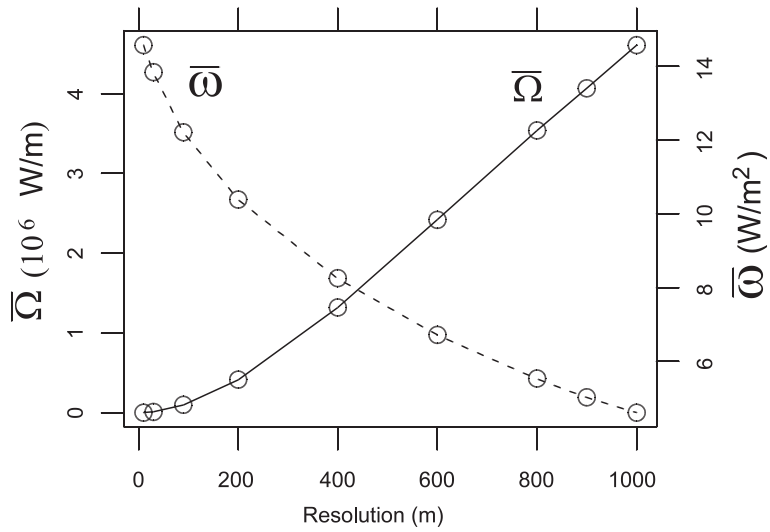

Fig. 11. Variation in mean stream power of the Elwha River as a function of grid resolution. Resolution is the length of one side of a square grid cell; hence, a "10-m" grid cell has a surface area of 100 m^2. Mean stream power per grid cell ($\overline{\Omega}$) increases with grid size while mean stream power per unit area ($\overline{\omega}$) decreases with increasing grid size. The low-resolution DEMs used in each stream power calculation were derived from the 10-m DEM.

calculations carried out at different resolutions cannot be compared to one another directly.

5. Conclusion

The problem of selecting a suitable erosion model that can scale to continental landscapes is not easily resolved. Stream power formulations typically account only for variation in stream discharge and slope. They do not account for a variety of factors that inhibit bedrock erosion, such as changes in lithology, in-stream momentum loss due to bed forms, or the need to mobilize bed cover. Nor do they account for seasonal differences in rainfall that statistical models suggest is an important factor in the variation of sediment yield of modern rivers (Eq. (1)). Lastly, it is not clear how to scale Stream Power Laws to continental analyses. Most attempts to parameterize stream power models have been performed on comparatively small watersheds.

In analyses of continental-scale areas, the two-dimensional raster grid of digital elevation models can cause severe distortion in distance and area measurements if an appropriate map projection is not carefully selected. Also, the grid size selected has an effect on mean slope, drainage basin size, and stream length. Slopes tend to decrease with increasing grid size, drainage basins tend to be larger, and stream length decreases significantly.

The Stream Power Law itself has a number of issues when scale is considered. The first is the application of the area-discharge proxy assumed in most discussions of stream power. We have presented evidence that for small river systems, the area-discharge proxy appears to be appropriate; but for large, continental-scale systems like the Indus River, the area-discharge proxy can mischaracterize the general pattern of discharge in the river. We are aware of similar patterns throughout the major river systems of the Himalaya, and it is likely that other continental rivers flowing through major climatic zones have similar problems with the area-discharge proxy. We present a simple, computationally efficient model for accounting explicitly for the spatially variable rainfall on the downstream structure of discharge accumulation. The parameterization of k, m and n in the stream power equation is very sensitive to slight changes in the best-fit line through an area-slope plot. Hence, as the number of sample points in a river long profile decreases with decreasing resolution, a bias in the regression can result. In our example, the bias in-

creased θ values and decreased k_s values. Moreover, the general decease in grid slope as grid resolution decreases is coupled to a decrease in mean stream power per unit area. Taken together, these results show a grid scale dependence of stream power that indicates the need for caution when comparing stream power erosion models generated from different grid resolutions.

Our current ability to estimate rates at which rivers erode bedrock remains limited by both a lack of high-resolution data and incomplete understanding of how to scale-up the pertinent erosional processes and mechanisms. Although it is still very difficult to obtain high-resolution topographic data for most large mountain ranges, high-resolution data on climate, geology, and land cover are even more difficult to acquire. Large-scale erosion modeling in GIS is relatively new and suffers from a number of problems that are not well documented or completely identified, but the technology offers a powerful set of tools for developing geomorphic insight into the topographic evolution of mountain ranges.

Acknowledgements

Thank you to M. Bishop and A. Marcus for the constructive reviews. Funding was provided by NSF (EAR-0003561) and NASA (NAG 5-10342).

References

Ahnert, F., 1970. Functional relationships between denudation, relief, and uplift in large mid-latitude drainage basins. American Journal of Science 268, 243–263.

Brandon, M.T., Roden-Tice, M.K., Garver, J.I., 1998. Late Cenozoic exhumation of the Cascadia accretionary wedge in the Olympic Mountains, northwest Washington State. Geological Society of America Bulletin 110, 985–1009.

Buffington, J.M., Montgomery, D.R., 1997. A systematic analysis of eight decades of incipient motion studies, with special reference to gravel-bedded rivers. Water Resources Research 33, 1993–2029.

Buffington, J.M., Montgomery, D.R., 1999. Effects of hydraulic roughness on surface textures of gravel-bed rivers. Water Resources Research 35, 3507–3521.

Carlston, C.W., 1969. Downstream variations in the hydraulic geometry of streams: special emphasis on mean velocity. American Journal of Science 267, 499–509.

Chow, V.T., 1959. Open Channel Hydraulics. McGraw-Hill, New York, NY, p. 680.

Collins, D.N., 1996. Sediment transport from glacierized basins in the Karakoram Mountains. In: Walling, D.E., Webb, B. (Eds.), Erosion and Sediment Yield: Global and Regional Perspectives. International Association of Hydrological Sciences, vol. 236, pp. 85–96.

Comanor, K., Bart, N., Lettenmaier, D.P., 2000. Five-minute, 1/2 degrees, and 1 degrees data sets of continental watersheds and river networks for use in regional and global hydrologic and climate modeling studies: discussion. Water Resources Research 36, 3117–3120.

Costa, J.E., O'Connor, E.O., 1995. Geomorphically effective floods. In: Costa, J.E., Miller, A.J., Potter, K.W., Wilcock, P.R. (Eds.), Natural and Anthropogenic Influences in Fluvial Geomorphology. American Geophysical Union, Washington, DC, pp. 45–56.

Daly, C., Neilson, R.P., Phillips, D.L., 1994. A statistical-topographic model for mapping climatological precipitation over mountainous terrain. Journal of Applied Meterology 33, 140–158.

Dunne, T., Leopold, L.B., 1978. Water in Environmental Planning. Freeman and Company, New York.

Finlayson, D.P., Montgomery, D.R., Hallet, B., 2002. Spatial coincidence of erosional and metamorphic hot spots in the Himalaya. Geology 30, 219–222.

Garbrecht, J., Martz, L.W., 2000. Digital elevation model issues in water resources modeling. In: Maidment, D., Djokic, D. (Eds.), Hydrologic and Hydraulic Modeling Support with Geographic Information Systems. ESRI Press, Redlands, CA, pp. 1–27.

Grahm, S.T., Famiglietti, J.S., Maidment, D.R., 1999. Five-minute, 1/2 degrees, and 1 degrees data sets of continental watersheds and river networks for use in regional and global hydrologic and climate system modeling studies. Water Resources Research 35, 583–587.

Gurnell, A.M., Montgomery, D.R., 1999. Hydrological Applications of GIS. Wiley, New York, NY, p. 176.

Hammer, R.D., Young, F.J., Wollenhaupt, N.C., Barney, T.L., Haithcoate, T.W., 1995. Slope class maps from soil survey and digital elevation models. Soil Science Society of America Journal 59, 509–519.

Howard, A.D., 1998. Long profile development of bedrock channels: interaction of weathering, mass wasting, bed erosion, and sediment transport. In: Tinkler, K.J., Wohl, E.E. (Eds.), Rivers Over Rocks: Fluvial Processes in Bedrock Channels. American Geophysical Union, Washington, DC, pp. 297–319.

Howard, A.D., Kerby, G., 1983. Channel changes in badlands. Geological Society of America Bulletin 94, 739–752.

Hradílek, L., Hamilton, A.C., 1973. A systematic analysis of distortions in map projections. Lecture Notes No. 34. University of New Brunswick, Fredericton, N.B., Canada.

Jansen, J.M.L., Painter, R.B., 1974. Predicting sediment yield from climate and topography. Journal of Hydrology 21, 371–380.

Knighton, A.D., 1987. River channel adjustment—the downstream dimension. In: Richards, K.S. (Ed.), River Channels: Environment and Process. Blackwell, Oxford, UK, pp. 95–128.

Knighton, A.D., 1998. Fluvial Forms and Processes: A New Perspective. Arnold, London, p. 383.

Langbein, W.B., Schumm, S.A., 1958. Yield of sediment in relation to mean annual precipitation. Transactions-American Geophysical Union 39, 1076–1084.

Leemans, R., Cramer, W.P., 1991. The IIASA database for mean monthly values of temperature, precipitation and cloudiness of a global terrestrial grid. Tech. Rep. RR-91-18 IIASA, Laxenburg, Austria.

Leopold, L.B., Maddock, T., 1953. The Hydraulic Geometry of Stream Channels and Some Physiographic Implications. Professional Paper 252. US Geological Survey, Washington, DC.

Ludwig, W., Probst, J.L., 1998. River sediment discharges to the oceans: present-day controls and global budgets. American Journal of Science 298, 265–295.

Maidment, D., Djokic, D., 2000. Hydrologic and Hydraulic Modeling Support with Geographic Information Systems. ESRI Press, Redlands, CA, p. 216.

McDonnell Jr., P.W., 1979. Introduction to Map Projections. Marcel Dekker, New York.

Milliman, J.D., Syvitski, J.P.M., 1992. Geomorphic/tectonic control of sediment discharge to the ocean: the importance of small mountain rivers. Journal of Geology 100, 325–344.

Montgomery, D.R., Gran, K.B., 2001. Downstream variations in the width of bedrock channels. Water Resources Research 37, 1841–1846.

Montgomery, D.R., Balco, G., Willett, S.D., 2001. Climate, tectonics, and the morphology of the Andes. Geology 29, 579–582.

Pazzaglia, F.J., Brandon, M.T., 2001. A fluvial record of long-term steady-state uplift and erosion across the Cascadia forarc high, western Washington State. American Journal of Science 300, 385–431.

Roe, G.H., Montgomery, D.R., Hallet, B., 2002. Effects of orographic precipitation variations on the concavity of steady-state river profiles. Geology 30, 143–146.

Saunders, W., 2000. Preparation of DEMs for use in environmental modeling analysis. In: Maidment, D., Djokic, D. (Eds.), Hydrologic and Hydraulic Modeling Support with Geographic Information Systems. ESRI Press, Redlands, CA, pp. 29–51.

Sklar, L., Dietrich, W.E., 1998. River longitudinal profiles and bedrock incision models: stream power and the influence of sediment supply. In: Tinkler, K.J., Wohl, E.E. (Eds.), Rivers Over Rock: Fluvial Processes in Bedrock Channels. American Geophysical Union, Washington, DC, pp. 237–260.

Slack, J.R., Landwehr, J.M., 1992. Hydro-climatic data network (HCDN): a U.S. Geological Survey streamflow data set for the United States for the study of climate variations, 1974–1988. Open-File Report 92-129. US Geological Survey, Reston, VA.

Snyder, J.P., 1987. Map Projections—A Working Manual. Professional Paper 1395. US Geological Survey, Washington, DC.

Snyder, N.P., Whipple, K.X., Tucker, G.E., Merrits, D.J., 2000. Landscape response to tectonic forcing: digital elevation model analysis of stream profiles in the Mendocino triple junction region, northern California. Geological Society of America Bulletin 112, 1250–1263.

Stock, J., Montgomery, D.R., 1999. Geologic constraints on bedrock river incision using the stream power law. Journal of Geophysical Research 104, 4983–4993.

US Geological Survey (USGS), 1996. GTOPO30 Global Digital Elevation Model. Tech. Rep. EROS Data Center, Sioux Falls, SD.

Walker, J.P., Willgoose, G.R., 1999. On the effect of digital elevation model accuracy on hydrology and geomorphology. Water Resources Research 35, 2259–2268.

Walling, D.E., Webb, B.W., 1996. Erosion and sediment yield: a global overview. In: Walling, D.E., Webb, B.W. (Eds.), Proceedings of an International Symposium on Erosion and Sediment Yield: Global and Regional Perspectives. International Association of Hydrological Sciences, vol. 239. IAHS-Publications, Louvain, pp. 2–19.

Whipple, K.X, Tucker, G.E., 1999. Dynamics of the stream-power river incision model: implications for height limits of mountain ranges, landscape response timescales, and research needs. Journal of Geophysical Research 104, 17661–17674.

Wilson, L., 1973. Variations in mean sediment yield as a function of mean annual precipitation. American Journal of Science 273, 335–349.

Zhang, W., Montgomery, D.R., 1994. Digital elevation model grid size, landscape representation, and hydrologic simulations. Water Resources Research 30, 1019–1028.

Zhang, X., Drake, N.A., Wainwright, J., Mulligan, M., 1999. Comparison of slope estimates from low resolution DEMs: scaling issues and fractal method for their solution. Earth Surface Processes and Landforms 24, 763–779.